Wavy stripes and squares in zero-Prandtl-number convection

Pinaki Pal and Krishna Kumar
Physics and Applied Mathematics Unit, Indian Statistical Institute, 203 Barrackpore Trunk Road, Calcutta 700 108, India
(Received 21 March 2001; revised manuscripts received 7 December 2001; published 25 March 2002)

A simple model to explain the numerically observed behavior of chaotically varying stripes and square patterns in zero-Prandtl-number convection in Boussinesq fluid is presented. The nonlinear interaction of mutually perpendicular sets of wavy rolls, via higher-order modes, may lead to a competition between the two sets of rolls. The appearance of square patterns is due to a secondary forward bifurcation from a set of wavy rolls. The statistics of the spatially averaged energy signal shows a power-law behavior.

DOI: 10.1103/PhysRevE.65.047302 PACS number(s): 47.27.−i

The study of low-Prandtl-number thermal convection [1–10] has been long motivated by its importance in astrophysical [1,2] and geophysical [3] problems. It is also useful in the study of bifurcation mechanism [4–7], crystal growth [8], metallic liquids [9], and pattern-forming instabilities [10]. The hydrodynamics of thermal convection in Boussinesq fluids is governed by two nonlinearities. The first describes self-interaction $\boldsymbol{v}\cdot\boldsymbol{\nabla}\boldsymbol{v}$ of the velocity field $\boldsymbol{v}$, and the second $\boldsymbol{v}\cdot\boldsymbol{\nabla}\theta$ results from the advection of the temperature fluctuation θ by the velocity field. The second nonlinearity $\boldsymbol{v}\cdot\boldsymbol{\nabla}\theta$ may be neglected in the asymptotic limit of zero Prandtl number [2]. The linearly growing two-dimensional (2D) rolls then become the exact solution of the nonlinear hydrodynamical equations in the close vicinity of the instability onset, if *stress-free* boundary conditions are considered. A nonlinear superposition of mutually perpendicular sets of 2D rolls also fails to saturate the instability just above the onset [5] of zero-Prandtl-number (P) convection. This makes this limit interesting even from purely theoretical point of view. Thual [6], in a quite general 3D direct numerical simulations (DNS) of the hydrodynamical equations in the limit of zero P, showed for the first time the saturation of the solution. This DNS showed many interesting patterns including the possibility of square patterns for $1.05<r\ (=R/R_c)<1.7$, where the critical Rayleigh number $R_c=27\pi^4/4$. The mechanism of saturation of the convection just above the onset was captured in a simple dynamical system [7], which agreed well with the results of DNS in its validity range. This model suggested that 2D rolls underwent *self-tuned* nonlocal wavy instability, which prevents their temporal growth further. The wavy instability had a wavelength larger than the wavelength of 2D rolls. The model showed either chaos or nonsaturation, if the wavelength of the wavy perturbation was chosen same as that of 2D rolls. The mechanism of selection of square convective cells, as observed in the DNS of zero P Boussinesq equations, remains unexplained.

We present in this paper a simple dynamical system, which describes the nonlinear interaction between mutually perpendicular sets of wavy rolls of the same wavelength, and captures the mechanism of the selection of square patterns in zero-Prandtl-number Boussinesq fluid. We show that the generation of the vertical vorticity is important in addition to higher-order modes to provide nonlinear coupling among mutually perpendicular sets of rolls. This is qualitatively different from the case of high-Prandtl-number convection [11] where nonlinear interaction of two sets of straight rolls may give rise to square patterns even in the absence of the vertical vorticity. The mutually perpendicular sets of wavy rolls interact through distortions in the vertical velocity as well as the vertical vorticity. The nonlinear interaction gives rise to complex convective patterns. A chaotic sequence of wavy stripes along x axis, square patterns, and again wavy stripes along y axis is observed. The generation of square patterns from wavy rolls is via a secondary forward bifurcation. In addition, we also study the statistics of the spatially averaged total energy of the chaotically varying patterns. They show power-law behavior. The probability distribution of the time elapsed ΔT between two maxima of the averaged energy signal is sharply peaked at $\Delta T\approx 2$.

We consider a thin horizontal layer of fluid of thickness d, uniform kinematic viscosity ν, and thermal diffusivity κ confined between two conducting boundaries, and heated underneath. The fluid motion is assumed to be governed by zero-Prandtl-number Boussinesq equations [2,6], which may be put in the following dimensionless form:

$$\partial_t(\nabla^2 v_3)=\nabla^4 v_3+R\nabla_H^2\theta-\hat{\boldsymbol{e}}_3\cdot\boldsymbol{\nabla}\times[(\boldsymbol{\omega}\cdot\boldsymbol{\nabla})\boldsymbol{v}-(\boldsymbol{v}\cdot\boldsymbol{\nabla})\boldsymbol{\omega}], \tag{1}$$

$$\partial_t\omega_3=\nabla^2\omega_3+[(\boldsymbol{\omega}\cdot\boldsymbol{\nabla})v_3-(\boldsymbol{v}\cdot\boldsymbol{\nabla})\omega_3], \tag{2}$$

$$\nabla^2\theta=-v_3, \tag{3}$$

where $\boldsymbol{v}(x,y,z,t)\equiv(v_1,v_2,v_3)$ is the velocity field, $\theta(x,y,z,t)$ the deviation in temperature field from the steady conduction profile, and $\boldsymbol{\omega}\equiv(\omega_1,\omega_2,\omega_3)=\boldsymbol{\nabla}\times\boldsymbol{v}$ the vorticity field in the fluid. The Rayleigh number R is defined as $R=\alpha(\Delta T)gd^3/\nu k$, where α is the coefficient of thermal expansion of the fluid, g the acceleration due to gravity, and ΔT the temperature difference across the fluid layer. The unit vector $\hat{\boldsymbol{e}}_3$ is directed vertically upward. The stress-free conducting flat boundary surfaces imply $v_3=\partial_{33}v_3=\theta=0$ at $x_3=0,1$. The symbol $\nabla_H^2=\partial_{11}+\partial_{22}$ stands for the horizontal Laplacian.

We employ the standard Galerkin procedure to describe the convective patterns in the form of mutually perpendicular sets of wavy rolls, and the patterns resulting due to their nonlinear superposition. The spatial dependence of the vertical velocity and the vertical vorticity are expanded in

Fourier series, which is compatible with the stress-free flat conducting boundaries and periodic boundary conditions in the horizontal plane. As DNS [6] showed standing patterns, all Fourier amplitudes in the expansion are set to be real. The vertical velocity v_3 and the vertical vorticity ω_3 then read as

$$\begin{aligned} v_3 = & [W_{101}(t)\cos kx_1 + W_{011}(t)\cos kx_2]\sin \pi x_3 \\ & + W_{111}(t)\sin kx_1 \sin kx_2 \sin \pi x_3 \\ & + W_{112}(t)\cos kx_1 \cos kx_2 \sin 2\pi x_3 \\ & + [W_{211}(t)\cos 2kx_1 \cos kx_2 \\ & + W_{121}(t)\cos kx_1 \cos 2kx_2]\sin \pi x_3, \end{aligned} \tag{4}$$

$$\begin{aligned} \omega_3 = & Z_{100}(t)\cos kx_1 + Z_{010}(t)\cos kx_2 \\ & + Z_{111}(t)\cos kx_1 \cos kx_2 \cos \pi x_3 + [Z_{201}(t)\cos 2kx_1 \\ & + Z_{021}(t)\cos 2kx_2]\cos \pi x_3 + [Z_{102}(t)\cos kx_1 \\ & + Z_{012}(t)\cos kx_2]\cos 2\pi x_3 + Z_{210}(t)\cos 2kx_1 \cos kx_2 \\ & + Z_{120}(t)\cos kx_1 \cos 2kx_2. \end{aligned} \tag{5}$$

The convective temperature field θ can be computed easily from Eq. (3). The solenoidal property of the velocity and the vorticity fields determine their horizontal components. Projecting the hydrodynamical Eqs. (1) to (3) on these modes, we get a 15-mode dynamical system, which is explicitly given in the Appendix. This is a minimum-mode consistent model for investigating competition between two mutually perpendicular sets wavy rolls.

There is no fixed points in the form of 2D rolls in this model as growing straight rolls, with growth rate $\epsilon = 3\pi^2(r-1)/2$, are exact solutions of the system just above the onset of convection in the absence of the vertical vorticiy. It is easy to see, although not given explicitly here, that the growing 2D rolls even with second harmonics generated by the self interaction of the critical mode W_{101} are also exact solutions of the system. The square solutions, in the absence of the vorticity field, may be described by only three modes W_{101}, W_{011}, and W_{112}. The mode W_{211}, which is usually small, is ignored for this analytic argument. The square fixed points ($X_1^2 = X_2^2$) are then described by the root of the equation $X_1^2 = 3\pi^2(27r-500)(r-1)/5$. For $1 < r < 500/27$, there is no real root showing the non-existence of the square fixed points. Numerical integration of the six-mode model (see the Appendix) in the absence of the vertical vorticity but including the mode W_{211} does not show saturation of the instability. This shows the importance of the vertical vorticity for the exchange of energy between two sets of rolls.

We now numerically integrate this dynamical system to investigate the unsteady solutions. As we are interested in solutions near the instability onset, we set $k = k_c = \pi/\sqrt{2}$. For each value of r, we integrate with randomly chosen initial conditions for long periods to get rid of transients. We raise r in small steps of $\Delta r (= 0.01)$ and repeat the above procedure. We get chaotic solutions for $1.11 \leqslant r \leqslant 1.42$, which are in qualitative agreement with the DNS [6]. We observe wavy rolls oscillating chaotically for $r < 1.11$, and for $r \geqslant 1.11$ a chaotic sequence of wavy rolls along x axis, squares, and wavy rolls along y axis. We have also repeated the above procedure by lowering r in small steps. The model does not show any hysteresis. The bifurcation is forward.

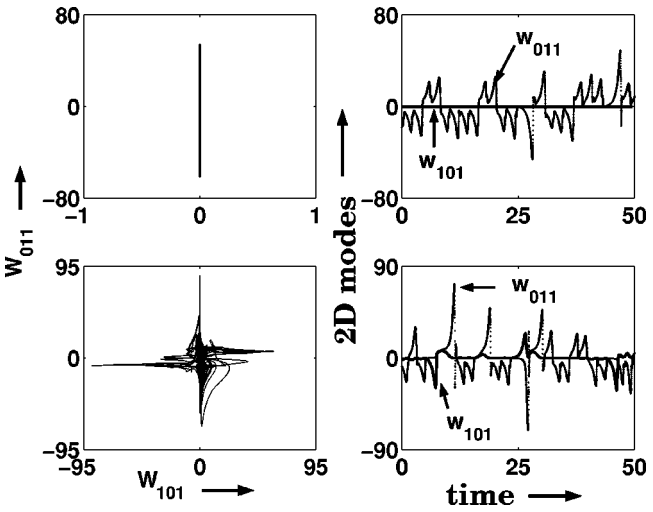

FIG. 1. Bifurcation from one set of chaotic rolls to two sets of chaotic rolls. The first column shows the projection of the phase space of the model on the $W_{011}-W_{101}$ plane for $r=1.10$ (above) and $r=1.11$ (below). The second column shows the variation of the 2D roll modes with time.

Figure 1 shows the bifurcation from one set of wavy rolls to two sets of wavy rolls. The competition between these two sets of mutually perpendicular rolls leads to chaotic sequence of patterns. The pictures in the first column show the projection of the phase space in $W_{011}-W_{101}$ plane for $r=1.10$ (top) and for $r=1.11$ (bottom). There is only one set of rolls for $r \leqslant 1.10$ and two sets of mutually perpendicular rolls for $r \geqslant 1.11$. The second column shows time evolution of 2D roll modes. While the mode W_{011} varies chaotically, the mode W_{101} remains zero for $r \leqslant 1.10$ (top). The dynamics is more complex for $r \geqslant 1.11$ (bottom) as two sets of wavy rolls are excited. The new 2D roll mode W_{101} excited at the onset of the secondary instability is also chaotic in time. This is an interesting example of forward bifurcation from one chaotic solution to another.

Figure 2 shows the time evolution of the chaotic patterns for $r \leqslant 1.10$. The thermal isotherms of the patterns show various structures in time, but they essentially remain along either x or y axis depending on the initial conditions. The curvature of the isotherms depends on the values of $W_{111}^2 + W_{211}^2$, which is a measure of the wave energy. Figure 3 shows various textures of the patterns just above the secondary instability at $r = 1.104 \pm 0.002$. Two sets of wavy rolls are competing via a nonlinear interaction between them. The isotherms of DNS [6] also show wavy character of the rolls. The oscillating square pattern is the result of the competition between two sets of rolls. Notice that the square pattern in Fig. 3 consists of two sets of squares. A small (big) square has four big (small) squares as its nearest neighbors. This feature of the square pattern is qualitatively new.

Figure 4 summarizes the results of the statistical analysis

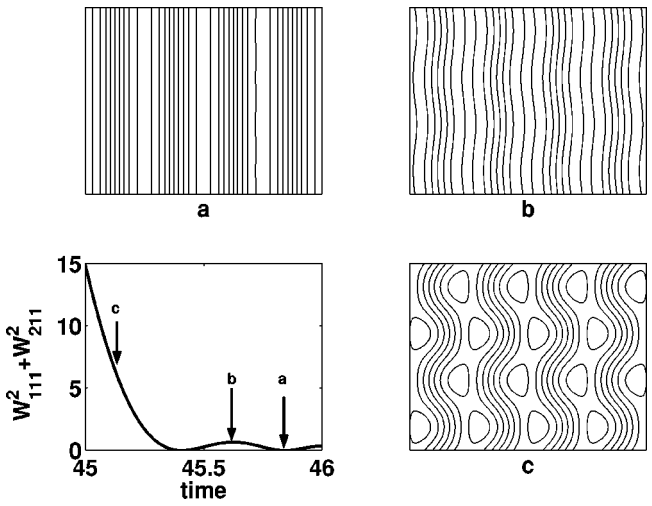

FIG. 2. Chaotic sequence (a)–(c) of isotherms for rolls with various wave energies at $r=1.10$. The variation of $W^2_{111}+W^2_{211}$, which is a measure of wavy energy, with dimensionless time is shown in the left lower box. The values of $W^2_{111}+W^2_{211}$ for the isotherms (a)–(c) are 0.0, 0.660, and 6.735, respectively.

of the energy signal of the model just above the onset of secondary instability. The spatially averaged total energy $\langle E\rangle$ (equal to $\frac{1}{2}\langle v_1^2+v_2^2+v_3^2\rangle_{x_1,x_2,x_3}$) is chaotic (top left) long after the transients die out. The signal shows the behavior of a chaotic relaxation oscillator. The histogram (top right) shows the variation of N_i, which is the number of times the ith energy bin with mean energy E_i has been visited by the spatially averaged energy signal, as a function of E_i. The signal for this purpose is recorded for a period approximately 2000 times the viscous time scale. We recorded four different signals generated with different initial conditions. In each case, data for transients for approximately 200 times the viscous time scale is dropped. The histogram shows non-Gaussian nature of the spatially averaged energy of the patterns. The frequency N_i scales with energy as $E_i^{-\alpha}$ with $\alpha=2.80\pm0.02$ (see right bottom of Fig. 4). Various symbols stand for four different energy signals. The probability distribution of the time elapsed Δt between two maxima of the energy signal is shown at the left bottom of Fig. 4. The probability distribution peaks at $\Delta t\approx 2$. This means that the system reaches its maximum energy state at almost regular intervals, although the maximum energy itself varies quite irregularly.

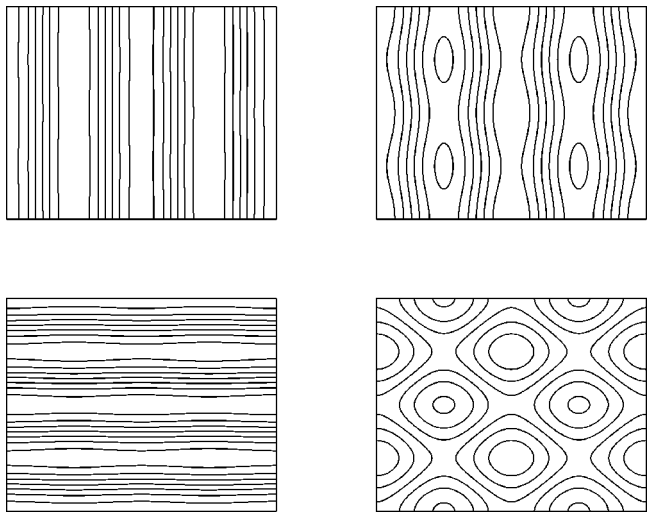

FIG. 3. Chaotic sequence of competing rolls and squares for $r=1.11$ arranged clockwise, starting from top left, with increasing time.

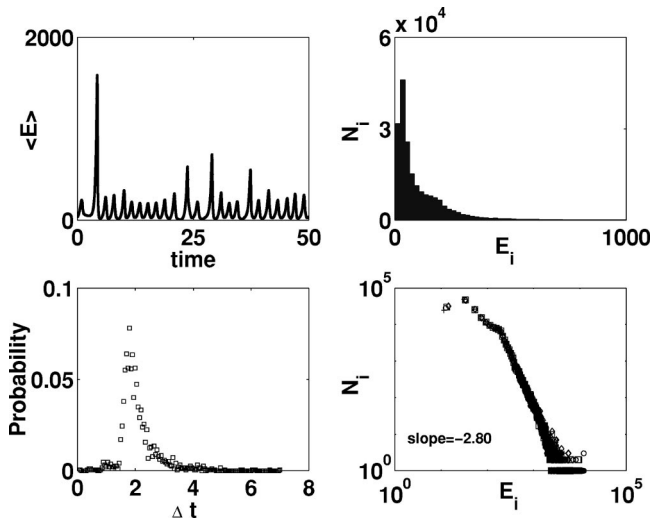

FIG. 4. Statistics of the total energy for $r=1.11$. The spatially averaged energy $\langle E\rangle$ (top left) shows chaotic variation long after transients die out. The histogram (top right) of a very long signal ($\approx$2000 viscous time scale) shows the strong non-Gaussian behavior. The slope of the power law regime is $=-2.80\pm.02$ (bottom right) for four different signals. The probability distribution of the time elapsed Δt between two maxima of the averaged energy of the patterns shows a sharp peak around $\Delta t\approx 2.0$ (bottom left).

We have presented in this paper a simple model that explains the mechanism responsible for generation of square patterns in zero-Prandtl-number Boussinesq fluids. As the Rayleigh number is raised above a critical value, one set of chaotic wavy rolls becomes unstable. Another set of wavy rolls is generated in a direction perpendicular to the former one. The nonlinear superposition of these two sets of wavy rolls gives rise to squares and other complex patterns. The secondary bifurcation is forward. The excitation of the vertical vorticity is responsible for the wavy nature of rolls. The wavy motion stops the unlimited growth of the patterns. The nonlinear modes, which depend on both the horizontal coordinates, facilitate the exchange of energy between two sets of wavy rolls. The spatially averaged total energy, varying chaotically as a relaxation oscillator, is highly non-Gaussian. It shows a power law behavior. Although the maximum energy of the system varies very erratically, the maximum energy state is reached by the system almost regularly.

We are thankful to S. Fauve (ENS, Paris) and M. K. Verma (IIT, Kanpur) for enlightening discussions. This work was supported by DST, India, under the project ''Pattern-forming instabilities and interface waves.''

APPENDIX: THE MODEL

$$\dot{\boldsymbol{X}}=\frac{3\pi^2}{2}(r-1)\boldsymbol{X}+\frac{\pi}{24}(\boldsymbol{X}^{\mathbf{i}}-\boldsymbol{Y})T-\frac{1}{30\pi}(10\boldsymbol{\zeta}+5\boldsymbol{\phi}+\boldsymbol{\psi})\eta-\frac{2}{15\pi}\begin{pmatrix}\chi_2\psi_2\\ \chi_1\psi_1\end{pmatrix}+\frac{1}{60}\begin{pmatrix}10\zeta_1+15\phi_1+3\psi_1\\ -10\zeta_2-15\phi_2-3\psi_2\end{pmatrix}S,$$

$$\dot{S}=\frac{\pi^2}{16}(27r-32)S-[(10\zeta_1+\psi_1+5\phi_1)(10X_1-3Y_2)+(10\zeta_2+\psi_2+5\phi_2)(10X_2-3Y_1)]/100,$$

$$\dot{T}=\frac{\pi^2}{100}(27r-500)T-\frac{\pi}{500}(300X_1X_2+63Y_1Y_2)+\frac{13\pi}{50}\boldsymbol{X}\cdot\boldsymbol{Y}+\frac{3}{40}(\chi_1-\chi_2)S-\frac{1}{10\pi}(\chi_1+\chi_2)\eta-\frac{2}{25\pi}[\psi_1\phi_2+\psi_2\phi_1+10(\zeta_2\phi_1-\zeta_1\phi_2)],$$

$$\dot{\boldsymbol{Y}}=\frac{\pi^2}{98}(135r-343)\boldsymbol{Y}-\frac{1}{70\pi}(5\boldsymbol{\phi}^{\mathbf{i}}+9\boldsymbol{\psi}^{\mathbf{i}}+10\boldsymbol{\zeta}^{\mathbf{i}})\eta+\frac{\pi}{280}(310\boldsymbol{X}+63\boldsymbol{Y}^{\mathbf{i}})T+\frac{3}{28}\begin{pmatrix}\phi_2+\psi_2+6\zeta_2\\ -\phi_1-\psi_1-6\zeta_1\end{pmatrix}S-\frac{2}{35\pi}\begin{pmatrix}4\chi_2\psi_1+5\chi_1\phi_1+10\zeta_1\chi_1\\ 4\chi_1\psi_2+5\chi_2\phi_2+10\zeta_2\chi_2\end{pmatrix},$$

$$\dot{\boldsymbol{\zeta}}=-\frac{\pi^2}{2}\boldsymbol{\zeta}+\frac{\pi}{80}\left[(10\boldsymbol{X}-\boldsymbol{Y}^{\mathbf{i}})\eta+20\boldsymbol{\phi}^{\mathbf{i}}T+\pi\begin{pmatrix}10X_1+3Y_2\\ -10X_2-3Y_1\end{pmatrix}S+2\begin{pmatrix}2\chi_1Y_1-5\chi_2X_2\\ 2\chi_2Y_2-5\chi_1X_1\end{pmatrix}\right],$$

$$\dot{\eta}=-2\pi^2\eta+\frac{\pi}{2}(2\boldsymbol{\zeta}+3\boldsymbol{\phi}-\boldsymbol{\psi})\cdot\boldsymbol{X}+\frac{\pi}{8}(\chi_1+\chi_2)T-\frac{\pi}{20}[(6\zeta_2-7\phi_2+\psi_2)Y_1+(6\zeta_1-7\phi_1+\psi_1)Y_2],$$

$$\dot{\boldsymbol{\psi}}=-\frac{5\pi^2}{2}\boldsymbol{\psi}+\frac{\pi}{40}\left[35\eta\boldsymbol{X}+50\boldsymbol{\phi}^{\mathbf{i}}T+\frac{13}{2}\eta\boldsymbol{Y}^{\mathbf{i}}+\frac{\pi}{2}\begin{pmatrix}9Y_2-10X_1\\ 10X_2-9Y_1\end{pmatrix}S+\begin{pmatrix}40\chi_1X_2+11\chi_2Y_1\\ 40\chi_2X_1+11\chi_1X_2\end{pmatrix}\right],$$

$$\dot{\boldsymbol{\phi}}=-\frac{9\pi^2}{2}\boldsymbol{\phi}+\frac{\pi}{4}(2\boldsymbol{\zeta}^{\mathbf{i}}-\boldsymbol{\psi}^{\mathbf{i}})T+\frac{\pi}{40}\left[\left(\frac{9}{2}\boldsymbol{Y}-5\boldsymbol{X}\right)\eta+\frac{\pi}{2}\begin{pmatrix}-10X_1-3Y_2\\ 10X_2+3Y_1\end{pmatrix}S+\begin{pmatrix}2\chi_1Y_1-15\chi_2X_2\\ 2\chi_2Y_2-15\chi_1X_1\end{pmatrix}\right],$$

$$\dot{\boldsymbol{\chi}}=-3\pi^2\boldsymbol{\chi}+\frac{\pi}{10}\begin{pmatrix}15\phi_2X_1+2\phi_1Y_1+\psi_2Y_2\\ 15\phi_1X_2+2\phi_2Y_2+\psi_1Y_1\end{pmatrix}+\frac{3\pi}{8}\begin{pmatrix}\eta-\pi S\\ \eta+\pi S\end{pmatrix}T+\frac{\pi}{5}\begin{pmatrix}5\zeta_2X_1+2\zeta_1Y_1\\ 5\zeta_1X_2+2\zeta_2Y_2\end{pmatrix},$$

where $\boldsymbol{X}\equiv(X_1,X_2)^{\mathbf{t}}=(W_{101},\ W_{011})^{\mathbf{t}}$, $\boldsymbol{Y}\equiv(Y_1,Y_2)^{\mathbf{t}}=(W_{211},W_{121})^{\mathbf{t}}$, $S=W_{111}$, $T=W_{112}$, $\boldsymbol{\zeta}\equiv(\zeta_1,\zeta_2)^{\mathbf{t}}=(Z_{010},Z_{100})^{\mathbf{t}}$, $\boldsymbol{\phi}\equiv(\phi_1,\phi_2)^{\mathbf{t}}=(Z_{012},Z_{102})^{\mathbf{t}}$, $\boldsymbol{\psi}\equiv(\psi_1,\psi_2)^{\mathbf{t}}=(Z_{210},\ Z_{120})^{\mathbf{t}}$, $\boldsymbol{\chi}\equiv(\chi_1,\chi_2)^{\mathbf{t}}=(Z_{201},\ Z_{021})^{\mathbf{t}}$, and $\eta=Z_{111}$. The superscript **t** stands for the transpose of a matrix. Any two column vectors $\boldsymbol{\Psi}^{\mathbf{i}}=(\Psi_2,\Psi_1)^{\mathbf{t}}$ and $\boldsymbol{\Psi}=(\Psi_1,\Psi_2)^{\mathbf{t}}$ have their elements interchanged.

[1] R.H. Kraichnan and E.A. Spiegel, Phys. Fluids **5**, 583 (1962); J. R. Herring, Woods Hole Oceanogr. Inst. Tech. Rep. No. WHOI-70-01, 1970 (unpublished); M.R. Proctor, J. Fluid Mech. **82**, 97 (1977).

[2] E.A. Spiegel, J. Geophys. Res. **67**, 3062 (1970).

[3] F. H. Busse, in *Fundamentals of Thermal Convection, Mantle Convection, Plate Tectonics and Global Dynamics*, edited by W. R. Peltier (Gordon and Breach, New York, 1989), pp. 23–95.

[4] R.M. Clever and F.H. Busse, J. Fluid Mech. **102**, 63 (1981); F.H. Busse and R.M. Clever, *ibid.* **102**, 75 (1981); P.L. Sulem, C. Sulem, and O. Thual, Prog. Astronaut. Aeronaut. **100**, 125 (1985); M. Meneguizzi, C. Sulem, P.L. Sulem, and O. Thual, J. Fluid Mech. **182**, 169 (1987); S. Fauve, E.W. Bolton, and M.E. Brachet, Physica D **29**, 202 (1987); V. Croquette, Contemp. Phys. **30**, 113 (1989); **30**, 153 (1989).

[5] K. Kumar, Woods Hole Oceanogr. Inst. Tech. Rep. No. WHOI-90-01, 1990 (unpublished).

[6] O. Thual, J. Fluid Mech. **240**, 229 (1992).

[7] K. Kumar, S. Fauve, and O. Thual, J. Phys. II **6**, 945 (1996).

[8] J.N. Koster, T. Seidel, and R. Derebail, J. Fluid Mech. **343**, 29 (1997); Y.-S. Lee and Ch.-H. Chun, J. Cryst. Growth **197**, 297 (1999).

[9] A. Chiffaudel, S. Fauve, and B. Perrin, Europhys. Lett. **4**, 555 (1987); J. Friedrich, Y.-S. Lee, B. Fischer, C. Kupfer, D. Vizman, and G. Müller, Phys. Fluids **11**, 853 (1999).

[10] R.M. Clever and F.H. Busse, Phys. Fluids A **2**, 334 (1990); M.C. Cross and P.C. Hohenberg, Rev. Mod. Phys. **65**, 851 (1993); Y.C. Hu, R. Ecke, and G. Ahlers, Phys. Rev. Lett. **72**, 2194 (1994); J. Liu and G. Ahlers, *ibid.* **77**, 3126 (1996); K. Kumar, S. Chaudhuri, and A. Das, Phys. Rev. E **65**, 026311 (2002).

[11] A. Das, U. Ghosal, and K. Kumar, Phys. Rev. E **62**, R3051 (2000).